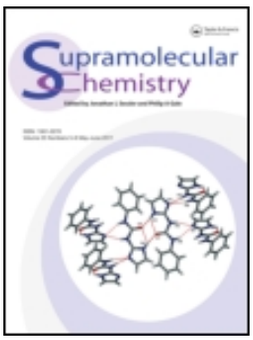

Supramolecular Chemistry

ISSN: 1061-0278 (Print) 1029-0478 (Online) Journal homepage: https://www.tandfonline.com/loi/gsch20

Inclusion by a xanthenol host: structures, kinetics of enclathration and desorption

Luigi R. Nassimbeni , Hong Su & Tanith-Lea Curtin

To cite this article: Luigi R. Nassimbeni , Hong Su & Tanith-Lea Curtin (2012) Inclusion by a xanthenol host: structures, kinetics of enclathration and desorption, Supramolecular Chemistry, 24:5, 344-349, DOI: 10.1080/10610278.2012.671484

To link to this article: https://doi.org/10.1080/10610278.2012.671484

Supramolecular Chemistry
Vol. 24, No. 5, May 2012, 344–349

Taylor & Francis
Taylor & Francis Group

Inclusion by a xanthenol host: structures, kinetics of enclathration and desorption

Luigi R. Nassimbeni*, Hong Su and Tanith-Lea Curtin

Department of Chemistry, University of Cape Town, Rondebosch, 7701 Cape Town, South Africa

(*Received 17 November 2011; final version received 6 February 2012*)

The host compound 9-(3-trifluoromethyl)-9H-xanthen-9-ol forms inclusion compounds with dimethylformamide, dimethylsulphoxide and 1,4-dioxane. The structures of the inclusion compounds as well as that of apohost have been elucidated. The kinetics of enclathration and of desorption have been analysed.

Keywords: inclusion compound; kinetics of desolvation and enclathration; structure

Introduction

Substituted xanthenols have proved to be versatile host molecules which form inclusion compounds with a variety of guests. The aristotype is 9-(4-methoxyphenyl)-9H-xanthen-9-ol which has been studied extensively. Its inclusion compounds with benzene, the isomers of xylene, cyclohexane, 1,4-dioxane and dimethylformamide have been elucidated (*1, 2*).

We have demonstrated the ability of this host to enclathrate solid guests made up of fused aromatic rings, namely naphthalene, anthracene, phenanthrene and pyrene by solid–solid grinding reactions. We evaluated the kinetics of the solid–solid reactions with naphthalene and β-naphthol by monitoring the change in the X-ray powder diffraction patterns (*3*).

The structures of the related host 9-(1-naphthyl)-9H-xanthen-9-ol with dioxane and its kinetics of desorption have been studied (*4*).

A comprehensive study of structure and selectivity has been carried out for the system comprising the host 9-(2-naphthyl)-9H-xanthen-9-ol with 1,4-dioxane, cyclohexanol and cyclohexanone, in which the stoichiometries of the inclusion compounds were reconciled with the structures (*5*).

We now present the structure of the apohost and the structures, kinetics of enclathration and kinetics of desorption of the inclusion compounds formed by the host 9-(3-trifluoromethyl)-9H-xanthen-9-ol (**H**) with dimethylformamide (**DMF**), dimethylsulphoxide (**DMSO**) and 1,4-dioxane (**DIOX**). The atomic numbering scheme is shown in Scheme 1.

Results and discussion

Structures

The crystal data, X-ray intensity data collection and refinement details are given in Table 1.

The apohost **H**, crystallised in the space group P $\bar{1}$ with $Z = 2$. The conformation of the molecule is governed by the torsion angle $O_{11}—C_9—C_{12}—C_{13}$ which has an absolute value of 11.2(2)° and thus shows the CF_3 moiety to be *cis*- to the hydroxyl group. This feature reoccurs in the host molecule of the subsequent structures. The structure is stabilised by hydrogen bonds formed between the hydroxyl moiety and the xanthenol oxygen of a neighbouring molecule, giving rise to a centrosymmetric dimer as shown in Figure 1. In this and other subsequent figures, only the hydroxyl hydrogens are shown, and the hydrogen bonds are displayed as dotted lines. The hydrogen bonding patterns are described in graph set notation (*6*). The packing, viewed along [100] is shown in Figure 2, which shows evidence of $\pi-\pi$ stacking interactions between the tricyclic ring moieties.

The **H·1/2DMF** structure crystallises in the space group P $\bar{1}$ with $Z = 4$. There are thus two independent host molecules and one guest in the asymmetric unit. Both CF_3 moieties are *cis* to their respective hydroxyl groups, and one of them is disordered over two positions. The hydrogen bonding, shown in Figure 3, shows (Host)-O—H···(Host)O—H···O = C(Guest) interactions. The metrics of the hydrogen bonding for this and the other structures are presented in Table 2. The guest **DMF** molecules lie in channels running in the [01 $\bar{1}$] direction.

The **H·1/2DMSO** structure crystallises in C2/c with $Z = 16$. The asymmetric unit contains two host molecules and one guest molecule, all located in general positions. The hydrogen bonding motif is the same as that exhibited by the **H·1/2DMF** structure, the packing is different, however, with pairs of **DMSO** molecules entrapped in centrosymmetric lacunae located at Wyckoff position *a*.

*Corresponding author. Email: luigi.nassimbeni@uct.ac.za

ISSN 1061-0278 print/ISSN 1029-0478 online

http://dx.doi.org/10.1080/10610278.2012.671484
http://www.tandfonline.com

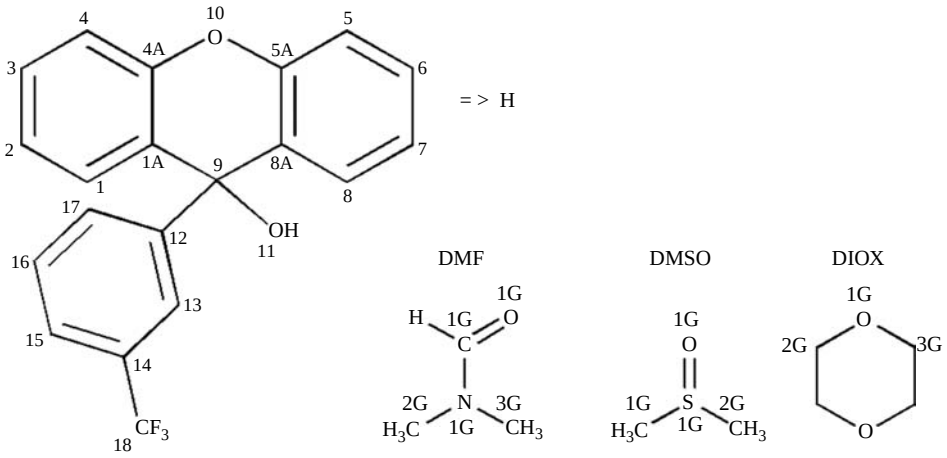

Scheme 1. Atomic numbering scheme for the host and guests.

Table 1. Crystallographic data for the structures under study. All data were collected at 113 (2) K.

	H	**H·1/2DMF**	**H·1/2DMSO**	**H·1/4DIOX**
Structure formula	$C_{20}H_{13}O_2F_3$	$C_{20}H_{13}O_2F_3{\cdot}C_{1.5}H_{3.5}N_{0.5}O_{0.5}$	$C_{20}H_{13}O_2F_3{\cdot}CH_3O_{0.5}S_{0.5}$	$C_{20}H_{13}O_2F_3{\cdot}CH_2O_{0.5}$
Formula weight	342.30	378.85	381.37	364.33
Space group	Triclinic, P $\bar{1}$	Triclinic, P $\bar{1}$	Monoclinic, C2/c	Monoclinic, $P2_1/n$
a (Å)	6.9755(1)	10.3718(2)	27.3535(3)	12.2364(1)
b (Å)	9.1408(2)	12.8768(2)	14.9040(3)	17.7528(2)
c (Å)	12.6032(2)	14.5872(2)	21.6745(4)	15.7612(1)
α (°)	108.473(1)	67.520(1)	90	90
β (°)	91.092(1)	89.467(1)	127.041(3)	102.192(1)
γ (°)	95.517(1)	86.448(1)	90	90
Volume (Å^3)	757.62(2)	1796.49(5)	7053.1(2)	3346.59(5)
Z	2	4	16	8
D_c/g cm^{-3}	1.501	1.401	1.437	1.446
μ (mm^{-1})	0.121	0.112	0.171	0.116
F (000)	352	784	3152	1504
Goodness of fit on F^2	1.051	1.105	1.139	1.238
R_1/wR_2 [I > 2σ(I)]	0.0366/0.0895	0.0474/0.1202	0.0417/0.1284	0.0580/0.1460
R_1/wR_2 (all data)	0.0438/0.0938	0.0606/0.1318	0.0513/0.1876	0.0786/0.1870

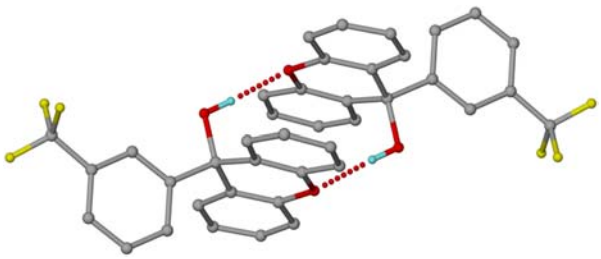

Figure 1. The host molecules form a dimer over an inversion centre via $R_2^2(12)$ hydrogen bonds.

The **H·1/4DIOX** structure crystallises in $P2_1/n$ with $Z = 8$. There are two host molecules in the asymmetric unit and the dioxane guest lies on a centre of inversion. The hydrogen bonds connect four host molecules and a dioxane guest as shown in Figure 4. The packing shows that the dioxane guest is trapped in cages, making this compound a true clathrate.

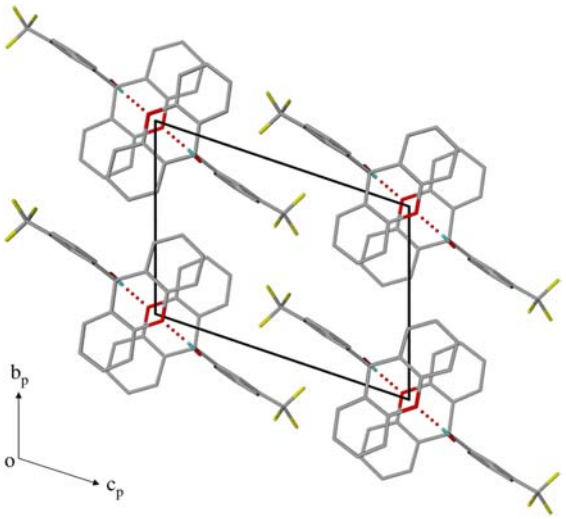

Figure 2. Projection of the apohost structure viewed down the *a*-axis.

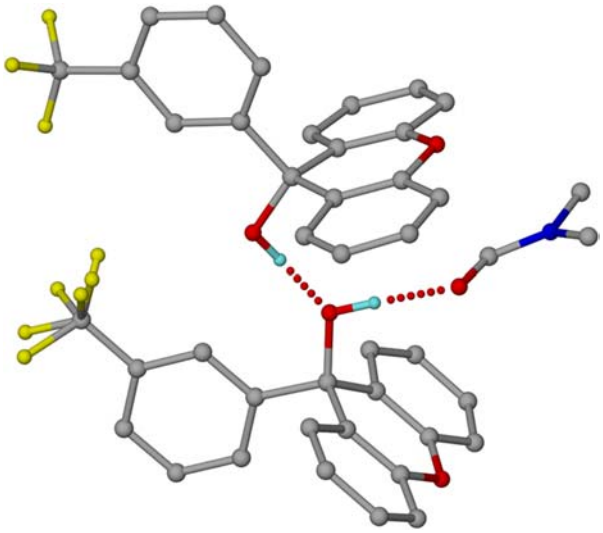

Figure 3. $D_2^2(5)$ H-bonding pattern for **H·1/2DMF**.

Kinetics

For solid–gas reactions between a solid host **H** and a gaseous guest **G**, which forms a solid inclusion compound:

$$\mathbf{H}(s) + nG(g) \underset{k_r}{\overset{kf}{\rightleftharpoons}} \mathbf{H} \cdot \mathbf{G}_n(s).$$

Several models for the kinetics are applicable for both the forward (enclathration) and the reverse (desorption) reactions (*7*). These models are based on various assumptions:

(1) Nucleation, in which the formation of nuclei is rate limiting, such as the power laws, the Avrami–Erofe'ev and the Prout–Tompkins equations.
(2) Geometrical contraction, in which the progress of the product layer from the surface to the inner particle governs the velocity of reaction. Examples are the contracting area and contracting volume equations.
(3) Diffusion, which can be 1D, 2D and 3D.
(4) Reaction order, where the rate laws are based on considerations derived from homogeneous reactions.

The Arrhenius equation

$$k = A \ \exp(-E_a/RT)$$

is often used to obtain values of the activation energy E_a and the pre-exponential factor A. The application of this equation to heterogeneous reactions is controversial, but Galway and Brown discuss this topic and give theoretical justification for its use (*8*, *9*). These parameters do not vary greatly with the kinetics model for the reaction when this is derived from isothermal data, but are model dependent for non-isothermal data (*10*).

Kinetics of enclathration

Kinetic studies were carried out with the special apparatus described in the experimental section. All the experiments were carried out at 25°C. The mass gain data were converted to the extent of reaction

$$\alpha = \frac{m_t - m_o}{m_\infty - m_o},$$

where m_o, m_t and m_∞ are the recorded masses at the start, during and end of the experiment, respectively. The α versus t curves can be fitted to various kinetic laws (*11*, *12*).

The results of the sorption runs are given in Table 3. In all three cases, the kinetic curves were deceleratory and obeyed the decreasing area model R2

$$kt = 1 - (1 - \alpha)^{1/2}.$$

The mass of guest absorbed corresponded to the stoichiometry of the inclusion compounds obtained as single crystals from solution, whose structures are described above. The powder X-ray diffraction patterns of the host–guest compounds thus obtained matched those calculated from the single-crystal structure analyses.

Kinetics of desorption

The kinetics of the desorption of both the **H·1/2DMF** and the **H·1/2DMSO** compounds were carried out by the non-isothermal technique of Flynn and Wall (*13*). Desorption curves were recorded at fixed rates β of 1, 2, 4, 8 and 16°C min^{-1}.

For the **H·1/2DMF** compound, plots of log β versus $1/T$ were recorded for various extents of reaction, α

Table 2. Hydrogen bonding details.

Inclusion compd.		D–H (Å)	H···A (Å)	D···A (Å)	<DHA (°)
H	O11–H11···O10$^{\#1}$	0.965(2)	1.910(2)	2.872(1)	175(2)
H·1/2DMF	O11X–H11X···O11Y	0.974(2)	1.765(2)	2.730(1)	170(1)
	O11Y–H11Y···O1G	0.994(2)	1.631(2)	2.624(1)	178(2)
H·1/2DMSO	O11X–H11X···O11Y	0.970(2)	1.791(2)	2.744(2)	167(1)
	O11Y–H11Y···O1G	0.995(2)	1.631(1)	2.619(2)	172(2)
H·1/4DIOX	O11X–H11X···O11Y	0.974(2)	1.761(2)	2.733(1)	175(2)
	O11Y–H11Y···O1G	0.973(2)	1.790(2)	2.744(2)	166(1)

Note: D, donor; A, acceptor; symmetry codes: #1 2–x, –y, 2–z.

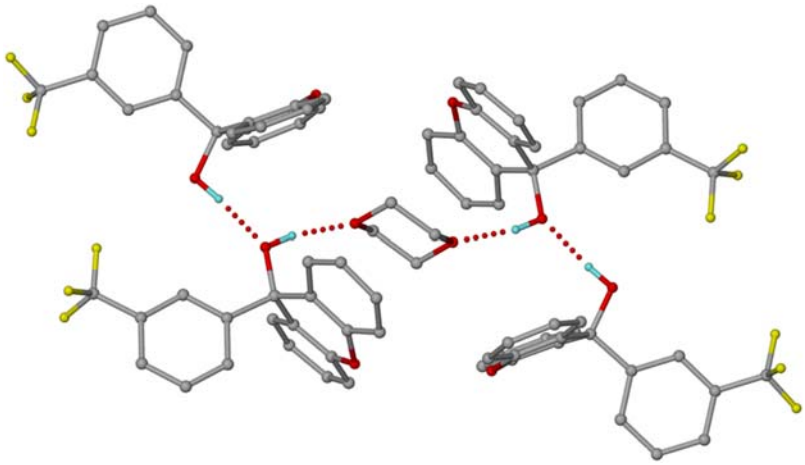

Figure 4. $D_4^4(12)$ H-bonding pattern for **H·1/4DIOX**.

Table 3. Sorption kinetics at 25°C.

Guest	α-range	k/min^{-1}	$t_{1/2}$/min	r
DIOX	0.05–0.90	9.19×10^{-2}	3.2	0.9991
DMF	0.05–0.90	1.55×10^{-2}	18.9	0.9972
DMSO	0.05–0.90	6.80×10^{-2}	4.3	0.9990

ranging from 5.2% to 20.7%. The results are shown in Figure 5, and yielded an activation energy ranging from 112(3) to 118(3) kJ mol^{-1}.

The results for the desorption of the **H·1/2DMSO** compound, whose semi-logarithmic plot is shown in Figure 6, yielded a similar activation energy ranging from 113(2) to 115(2) kJ mol^{-1} for α varying from 4.4% to 17.5%.

The desorption of the **H·1/4DIOX** compound was carried out isothermally at four different temperatures viz 72, 76, 80 and 84°C. All four kinetic curves were deceleratory and fitted the decreasing area model R2.

The rate constants k are reported in Table 4. The semi-logarithmic plot of ln k versus $1/T$ is shown in Figure 7, and yielded an activation energy of 148(7) kJ mol^{-1}.

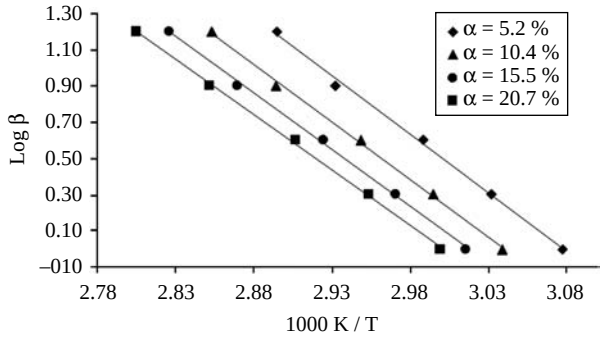

Figure 5. Kinetics of desorption for **H·1/2DMF**.

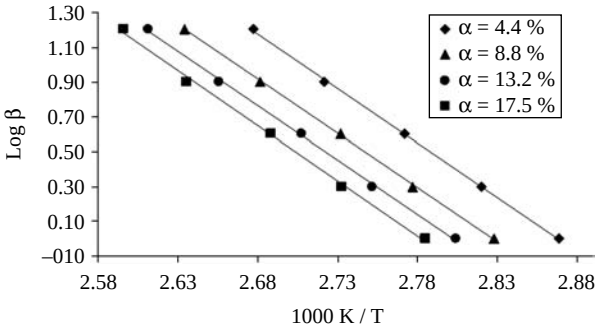

Figure 6. Kinetics of desorption for **H·1/2DMSO**.

The kinetics of decomposition of similar xanthenol inclusion compounds have been studied. The host 1,4-hydroxyl-1,4-toluenyldibenzo[a:j]xanthene enclathrates dimethyl formamide and its desorption follows first-order kinetics with an activation energy of 94 kJ mol^{-1} (*14*). The related host 9-(2-naphthyl)-9H-xanthen-9-ol forms inclusion compounds with cyclohexanol and cyclohexanone and their activation energies of desorption yielded values in the ranges of 91–104 kJ mol^{-1} and 77–92 kJ mol^{-1}, respectively (*5*). The kinetics of guest exchange and desolvation have been reported for the host 9-(4-methoxyphenyl)-9H-xanthen-9-ol. The desolvation reaction of the **DMF** inclusion compound followed the deceleratory contracting volume model R3, with an activation energy of 143(5) kJ mol^{-1}, while the dioxane

Table 4. Desorption kinetics of **H·1/4DIOX**.

Temperature/°C	α-range	k/min^{-1}	r
72	0.05–0.95	7.426×10^{-3}	0.9992
76	0.05–0.95	1.483×10^{-2}	0.9996
78	0.05–0.95	2.364×10^{-2}	0.9998
84	0.10–0.90	4.361×10^{-2}	0.9996

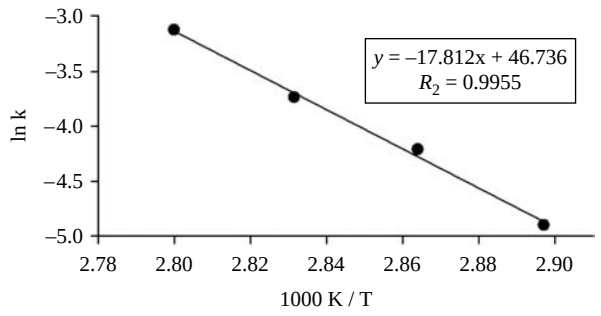

Figure 7. Isothermal kinetics of desorption for **H·1/4DIOX**.

inclusion compound gave activation energies in the range of 133–162 kJ mol^{-1} (*2*).

Experimental

Structure analysis

Crystals of **H·1/2DMF**, **H·1/2DMSO** and **H·1/4DIOX** were grown by slow evaporation of dilute solutions of the host in their respective guests. Crystals of the apohost were grown from toluene. Cell dimensions were established from the intensity data measured on a Nonius Kappa CCD diffractometer using graphite-monochromated M_o–K_α radiation. The strategy for the data collection was evaluated using the COLLECT software (*15*), and for all structures, the intensity data were collected by the standard phi scan and omega scan techniques and scaled and reduced using the program DENZO-SMN (*16*). The structures were solved by direct methods and refined by full-matrix least squares on F^2 using SHELX-97 program packages (*17*). The program X-seed (*18*) was used as a graphic interface. All the non-hydrogen atoms were positioned using direct methods and refined anisotropically; the hydroxyl hydrogens of the host were located in difference electron density maps and refined with bond length constraints according to a function of O—H versus O···O distances based on neutron diffraction data (*19*). The other hydrogen atoms were in fixed positions and were refined as riding on their parent atoms with isotropic temperature factors.

Crystallographic data for the structures in this paper have been deposited with the Cambridge Crystallographic Centre as supplementary publication number 837619–837622. Copies of data can be obtained, free of charge, on application to the Director, CCDC, 12 Union Road, Cambridge, CB2 1EZ, UK (Fax: +44-1223-336033, deposit@ccdc.cam.ac.uk).

Kinetics of desorption

The thermal gravimetry (TG) data were collected on a TGA Q500 (TA instruments), with a purge gas of dry nitrogen flowing at 50 ml min^{-1}.

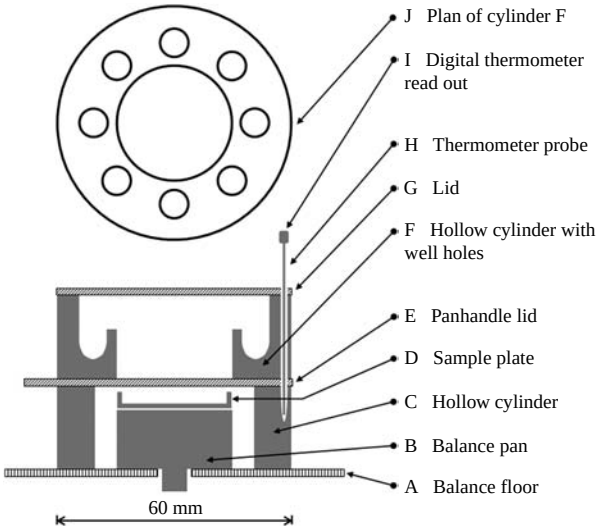

Figure 8. The apparatus for kinetics of enclathration.

The kinetics of enclathration were carried out with a special device described below:

The apparatus is shown in Figure 8, and all parts are made of brass. The balance pan is replaced by a smaller pan B, which is surrounded by a cylinder C. The host compound is placed in sample plate D and is immediately covered by a pan-handle plate E. The volatile liquid guest is pipetted into the well holes of the hollow cylinder F, is covered by the lid G and placed on lid E. A digital thermometer I is inserted into the hole. The balance is located in a thermostated cupboard. When the brass apparatus has equilibrated to the desired temperature (typically 15 min), the balance is tared, plate E is removed, and the guest vapour quickly expands into the lower cylinder and comes into contact with the host powder. The kinetic run is started and the increase in mass as a function of time is recorded automatically on a computer.

We note that this apparatus allows the kinetics to be measured at ambient conditions where the host powder is exposed to the vapour pressure of the guest as well as the air molecules under the total atmospheric pressure.

Conclusion

The structures of a xanthenol apohost and of its inclusion compounds with dimethylformamide, dimethylsulphoxide and 1,4-dioxane have been elucidated. The conformation of the host compound remains essentially unchanged, and hydrogen bonding stabilises all four structures. The kinetics of desorption of the inclusion compounds yield activation energies in the range of 112–148 kJ mol^{-1}. A simple apparatus is described which allows the measurement of the kinetics of enclathration under ambient conditions. The half lives for the latter reactions varied from 3.2 to 18.9 min at 25°C.

References

(1) Jacobs, A.; Nassimbeni, L.R.; Su, H.; Taljaard, B. *Org. Biomol. Chem.* **2005**, *3*, 1319–1922.
(2) Jacobs, A.; Faleni, N.; Nassimbeni, L.R.; Taljaard, J.H. *Cryst. Growth Des.* **2007**, *7*, 1003–1006.
(3) Curtis, E.; Nassimbeni, L.R.; Su, H.; Taljaard, T.H. *Cryst. Growth Des.* **2006**, *6*, 2716–2719.
(4) Jacobs, A.; Nassimbeni, L.R.; Taljaard, B. *Acta Cryst.* **2004**, *C60*, 668–670.
(5) Jacobs, A.; Nassimbeni, L.R.; Nohako, K.L.; Su, H.; Taljaard, J.H. *Cryst. Growth Des.* **2008**, *8*, 1301–1305.
(6) Etter, M.C.; MacDonald, J.C.; Bernstein, J. *Acta Cryst.* **1990**, *B46*, 256–262.
(7) Galwey, A.K.; Brown, M.E. In *Handbook of Thermal Analysis and Calorimetry*; Brown, M.E., Ed.; Elsevier Science B.V: Amsterdam, 1998; Vol. 1.
(8) Brown, M.E.; Galway, A.K. *Anal. Chem.* **1989**, *61*, 1136–1139.
(9) Galway, A.K.; Brown, M.E. *Proc. R. Soc. Lond.* **1995**, *450*, 501–512.
(10) Zhou, D.; Grant, D.J.W. *J. Phys. Chem. A*. **2004**, *108*, 4239–4246.
(11) Khawan, A.; Flanagan, D.R. *J. Phys. Chem. B*. **2006**, *110*, 17315–17328.
(12) Khawan, A.; Flanagan, D.R. *J. Pharm. Sci.* **2006**, *95*, 472–498.
(13) Flynn, J.H.; Wall, L.A. *Polymer Lett.* **1966**, *4*, 323–328.
(14) Jacobs, A.; Makgosi, S.M.; Nassimbeni, L.R.; Taljaard, J.A. *J. Chem. Cryst.* **2009**, *39*, 163–168.
(15) COLLECT, data collection software: Nonius BV Delft: The Netherlands, **2000**.
(16) Otwinowski, Z.; Minor, W. *Methods Enzymol.* **1997**, *276*, 307.
(17) Sheldrick, G.M. *SHELXL-97: Programe for the Refinement of Crystal Structures*; University of Göttingen, 1997.
(18) Barbour, L.J. *J. Supramol. Chem.* **2001**, *1*, 189–191.
(19) Olovsson, I.; Jönson, P. In *The Hygrogen Bonds – Structure and Spectroscopy*; Schuster, P., Zundel, G., Sarderfy, C., Eds.; North-Holland Publishing Company: New York, 1975.